www.czasopisma.pan.pl PAN POLSKA AKADEMIA NAUK www.journals.pan.pl

Arch. Metall. Mater. **67** (2022), 2, 759-766

DOI: https://doi.org/10.24425/amm.2022.137815

MASAHIKO HATAKEYAMA[1*], YUSUKE SHIMADA[2], NAOKI KAWATE[2], KAEDE SARAYAMA[2], SATOSHI SUNADA[1]

THE ROLE OF β($Al_{12}Mg_{17}$) PHASE ON CORROSION BEHAVIOR OF THE AM90 ALLOY IN NaCl AQUEOUS SOLUTION

The β phase ($Al_{12}Mg_{17}$) precipitated by heat treatment in some alloy compositions may result deterioration of corrosion resistance. However, much of its role remains unclear. The effect of the β phase on the corrosion resistance behavior in a NaCl solution was presented in this study. The specimen was Mg-9mass%Al (AM90) alloy and the content of the β phase precipitant was controlled systematically by aging time at 473 K. Area rate of β and lamellar phase in the specimens were 0, 10 and 100%, respectively. According to the results of cathodic polarization curves measurement, the corrosion current density of α phase was 0.215 A/m^2 and β phase of it was 0.096 A/m^2. While, the specimen includes 10% of β and lamellar phase showed large corrosion current density of 0.251 A/m^2. Positive correlation between the β phase and the open circuit potential, suggest that the β phase acts as a cathodic electrode. Moreover, the microstructure after postentiostatic corrosion tests was also support the role of β phase.

Keywords: magnesium; corrosion; light alloy

1. Introduction

Magnesium alloy is widely used as a structural material for many transportation devices and mobile devices due to its lightweight property, however its poor corrosion resistance is a bottleneck for further expansion of usage, and it is an urgent need to improve its corrosion resistance. Investigations on a wide variety of magnesium alloys are in progress [1-7].

AM series Mg-Al binary alloy is shifted to noble side by adding Al and has a relatively high corrosion resistance among magnesium alloys. In general, it is thought that increasing Al concentrations in Mg-Al alloys have a beneficial effect on the corrosion behavior in NaCl solutions [8,9]. It is mainly and widely used as the casting alloy. However, increasing of Al concentrations enhance the formation of β phase composed of $Mg_{17}Al_{12}$ during cooling process on casting. In the case of high cooling rate, the β phase is formed as dispersed coarse precipitates, and often exhibits pitting corrosion considered to be Galvanic corrosion at the surrounding α phase in NaCl solutions. In the case of AZ91D, it is suggested that β phase act as cathodic electrode [10-12]. On the other hand, for a high volume fraction, β phase might act as an anodic barrier to inhibit the overall corrosion of the alloy [13]. Therefore, there is controversy about its role in the corrosion behavior of Mg-Al alloys [14].

In recent years, by adding NaOH to control pH to a strong alkali, the reliability of the measurement accuracy of electrochemical tests of magnesium alloys has improved [15]. Hence, detailed polarization tests can be obtained even with AM and AZ series magnesium alloys. However, even recently, data such as corrosion potential and corrosion current density of a single β phase are insufficient, and their values are also controversial [16,17]. E. Koç reported the potential of –1.286 V/SCE, while S. Al. Bacha et al. reported –1.20 V/SCE in the same environment of 3.5 wt% NaCl solution. Although, Grimm et al. reported the corrosion potentials of various Al content AM series alloys, the corrosion potential of β phase was not described in the paper [18]. Therefore, the effect of the volume fraction of β phase on the corrosive properties of AM series alloy in the same environment has not been sufficiently investigated.

We have previously reported in this journal that the effect of the volume fraction of β phase on the corrosion behavior of AZ91, which is containing Zn [12]. Since the corrosive properties

[1] UNIVERSITY OF TOYAMA, GRADUATE SCHOOL OF MATERIALS SCIENCE AND ENGINEERING FOR RESEARCH, 3190 GOFUKU, TOYAMA 930-8555, JAPAN
[2] UNIVERSITY OF TOYAMA, GRADUATE SCHOOL OF MATERIALS SCIENCE AND ENGINEERING FOR EDUCATION, JAPAN

* Corresponding author: hatake@sus.u-toyama.ac.jp

of the β phase of the AM series also seem to be more important, similar electro chemical experiments were carried out on the AM90 alloy in this study.

The influence of the volume fraction of β phase on the corrosion resistance behavior in a NaCl solution was studied in this work. The specimen was Mg-9mass%Al alloy and the content of the β phase precipitant was controlled systematically by heat treatments. Electrochemical measurements were carried out on the specimens.

2. Specimens and experiments

2.1. Preparation of the specimen

The test material was fabricated by casting to obtain Mg-9mass%Al alloy. Mg ingot with industrial purity, pure Al ingot, pure Mn flakes and Al-2.5mass% Be mother alloy were prepared, the latter was cut from ingot to make a final total weight as 400 gf. Pure Mg ingot was melted at 1023 K while fire prevention gas composed of CO_2 and 2%SF_6 was blown to the molten surface. Al ingot was added at the same temperature followed by further addition of pure Mn flakes and Al-2.5mass% Be mother alloy in this order to a predetermined amount while keeping the temperature at 993 K. Molten alloy was fed into the casting mold and a Y-shaped casting block was obtained. Specimens with a dimension of 15×12×2 mm were cut from the Y-shaped cast block. Solution treated specimens were obtained after heat treatment of 172.8 ks at 703 K on the cast specimens. The aging curves of Mg-9mass%Al alloys is shown in Fig. 1. Two kinds of aging treated specimens were obtained after aging treatment for 2.7 ks and 86.4 ks respectively on the solution treated specimens using an oil bath kept at 473 K. A total of four kinds of specimens with different microstructure were prepared for evaluations; the as-cast, the solution treated, the sub-aged for 2.7 ks and the peak-aged for 86.4 ks specimens. The composition of the specimen is given in TABLE 1. A 0.176 mol/dm^3 NaCl solution was prepared as the test solution.

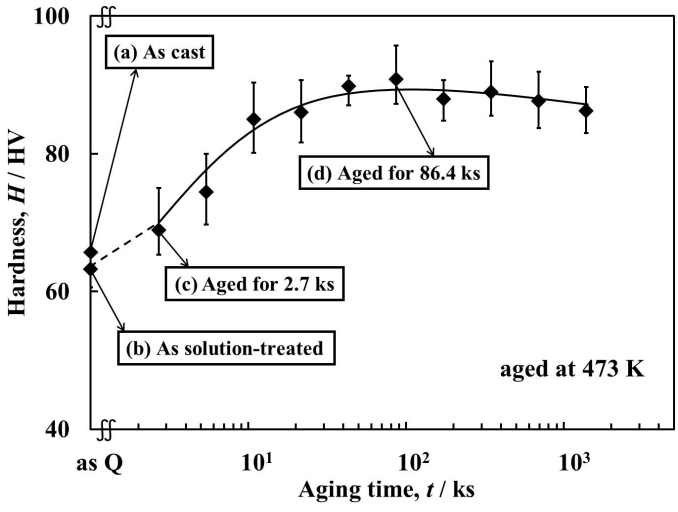

Fig. 1. The aging curves of Mg-9mass%Al alloys

TABLE 1

Chemical composition of the AM90(mass%)

Element	Al	Zn	Mn	Si	Fe	Cu	Mg
AM90	8.1	0.006	—	0.011	0.003	0.001	Bal.

Electrochemical measurements were made for the as-cast, the solution treated, the sub-aged and the peak-aged specimens. The reaction surface of the specimen was polished with fine abrasive papers of 80 to 2000 grades followed by defatting with acetone, cleaning and drying. The surface was coated with silicone rubber for isolation except a reaction area of 1.0×10^{-4} m^2 and used as a test electrode.

2.2. Observation of microstructure using optical microscope

Prepared each specimen was polished with fine abrasive papers of 80 to 2000 grades at first, then buff polished with diamond paste and finally etched. Etching reagent for the as-cast specimens was mixture of 1% nitric acid and 99% ethanol. Mixed solution of picric acid was used for the heat treated specimens. Microstructures were observed with an optical microscope BX51M made by OLYMPUS.

2.3. Open circuit potential measurements

It was reported that an oxide film is formed on the surface of magnesium alloy immediately after revealing fresh surface by polishing and the thickness of the film increases with immersion time. Then, influence of the immersion time on the corrosion characteristics of the specimen surface was investigated by measuring changes of the Open circuit potential (OCP) over time. Namely, in the measurement of time dependence of the OCP, a corrosive solution fully deoxidized with pure N_2 gas was prepared. A volume of 2×10^{-4} m^3 of it was filled into an electrolytic cell contained in an isothermal bath kept at 289 K, then the potential E_{corr} was measured with a potentiostat during 72 hrs. High pure N_2 gas was continuously ventilated in the test environment. An Ag/AgCl electrode (3.33 kmol·m^{-3} KCl) was used as a referential electrode. Potentials cited in this work were referred to the Ag/AgCl electrode potential.

2.4. Polarization curve measurements

A polarization curve was measured for each specimen to investigate electrochemical characteristics of the Mg-9mass%Al alloy. An electrolytic cell used for polarization measurements was a H-shaped cell with an internal volume of 4×10^{-4} m^3. The arrangement was a typical three-electrode cell with a specimen electrode having a reaction area of 1.0×10^{-4} m^2 as the working electrode, a Pt counter electrode and a Ag/AgCl(3.33 kmol·m^{-3} KCl)

electrode as reference. An electrolytic cell kept at 298 K was deaerated by pure N_2 gas flow during 30 minutes. A potentiodynamic scanning was carried out with a rate of 0.5 mVs^{-1} started from near the OCP (E_{corr}) in potential ranges between –1.6 V and –1.0 V at an anode side and between –1.45 V and –2.0 V at a cathode side, in order to obtain accurate polarization curve in magnesium alloys. Measured potentials and current densities were recorded after logarithmic conversion. Measurements for Mg alloys were started 1.8ks after dissolution to equalize initial conditions since the OCP (E_{corr}) of Mg alloy varies according to dissolution time.

2.5. Electrochemical impedance tests

Electrochemical impedance was measured to investigate corrosion characteristics obtained from polarization curves in more detail. The work station used in this experiment for electrochemical impedance measurements consisted with a HZ-3000 potentiostatic polarization circuit made by HOKUTODENKO and a 5080 frequency response analyzer (below is called FRA) made by NF corporation. A sine wave signal generated by the FRA was sent to a potentiostat, which send an alternating potential to the specimen electrode for potentiostatic polarization in turn. Both the alternating potential and the corresponding alternating current were processed digitally using Fourier integration to obtain the impedance and the phase difference. This series of processes to obtain impedance was carried out by the computer supplied with the FRA. In EIS measurements with controlled potential, potentials were set at E_{corr}, E_{corr} +20 mV, ±40 mV, +60 mV, ±100 mV, 150 mV and ±200 mV for each specimen of the three-electrode system based on the data of corrosion characteristics at a cathodic region and an anodic region obtained by polarization curves. EIS measurements were carried out with the step-up method where the potential is maintained for a specific time to compare corrosion characteristics for each set potential [19]. The set potential was maintained during 1.8 ks before the following EIS measurement to stabilize surface condition of the electrode, then, EIS was measured during 3.0 ks while maintaining the set potential. EIS measurements were carried out at a cathode side and an anode side separately. Sine wave alternating potential with amplitude of 10 mV was given to each set potential and EIS was measured at 5 different points during a frequency change of an order of magnitude in the frequency range from 100 kHz down to 1 mHz.

2.6. Potentiostatic corrosion tests with constant electric charges

Corrosion morphology after potentiosatic corrosion test was observed for each Mg-9mass%Al alloy specimen. The surface was corroded by a coulombmeter applying a quantity of electricity of 5×10^4 C/m^2 to the reaction surface of 1.0×10^{-4} m^2 while the set potential of each specimen was maintained at E_{corr} +0.1 V by the potentiostat. After the test, the specimen was cleaned with deionized water, dried in a vacuum desiccator and embedded in a resin. The cross-sectional microstructure of each specimen was observed by an optical microscope.

2.7. Cathodic polarization curve after application of 5 C/cm^2

In order to investigate the influence of the β phase, the specimen was polarized cathodically by applying 5 C/cm^2 charges to expose the β phase. The surface was corroded by a coulombmeter applying 5×10^4 C/m^2 charges to the reaction surface of 1.0×10^{-4} m^2 while the set potential of each specimen was maintained at E_{corr} +0.1 V by the potentiostat. Mg-9mass%Al alloy was corroded by applying a charge amount of 5 C/cm^2, then cathodic polarization was measured under the measurement condition mentioned above.

3. Results and discussion

3.1. Microstructural observation

Fig. 2 shows microstructure of four kinds of specimens; the as-cast, the solution treated, the sub-aged and the peak-aged specimens. The as-cast specimen shows white matrix of the primary crystal α phase and the precipitated β phase particles are observed at the grain boundaries. The solution treated specimen after heat treatment of solution shows only the α phase since the precipitated β phase particles are dissolved into the α phase matrix in full. The sub-aged specimen for 2.7 ks shows only cellular precipitants. In the aged specimen for 86.4ks, specimen surface is occupied with both grown cellular precipitants and intragranular precipitates which were reported as lamellar precipitates [20,21] precipitated within crystal grains. Area rate of the β and lamellar phase was calculated as 12% for the as-cast, 0% for the solution treated, 10% for the sub-aged and 100 % for the peak-aged specimens when an area of the β phase was considered as a total area of precipitated β phase, lamellar precipitants and intragranular precipitation.

3.2. OCP measurements

OCP was measured during 72 hrs. in a 0.176 mol/dm^3 NaCl solution to find a requirement to obtain an equal initial surface morphology before the measurements of the polarization curve and the EIS. Fig. 3 shows time dependence of the OCP for each specimen. All four specimens show rapid rises of the OCP after immersion. After 8 ks, potentials stabilize gradually and rise monotonously. Hara reported that a surface film is formed immediately after an exposure of a fresh surface by polishing and the film thickness increases with immersion time [22]. It is shown

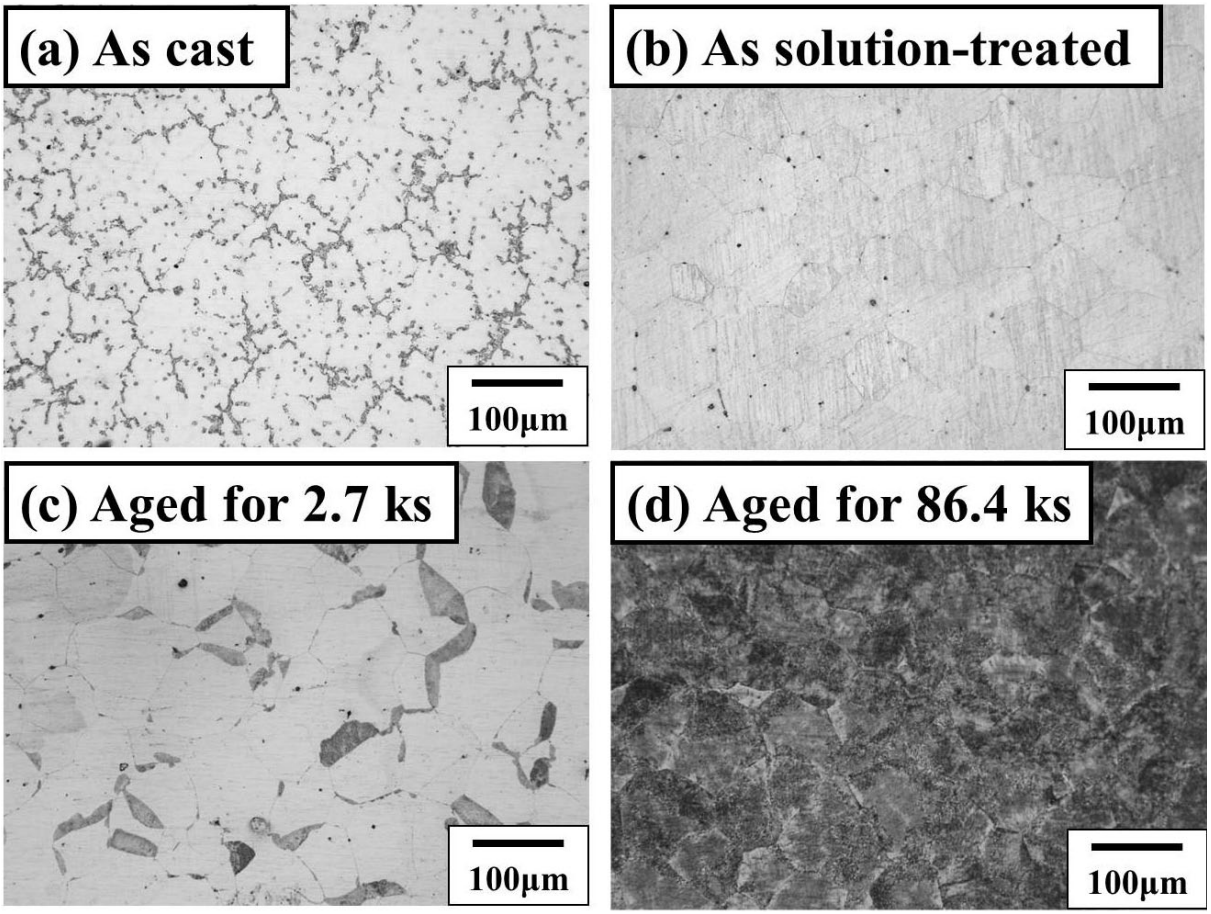

Fig. 2. Microstructure of the Mg-9mass%Al alloys of (a) as cast, (b) solution treated (c) 2.7 ks-aged, (d) 86.4 ks-aged at 473 K, respectively

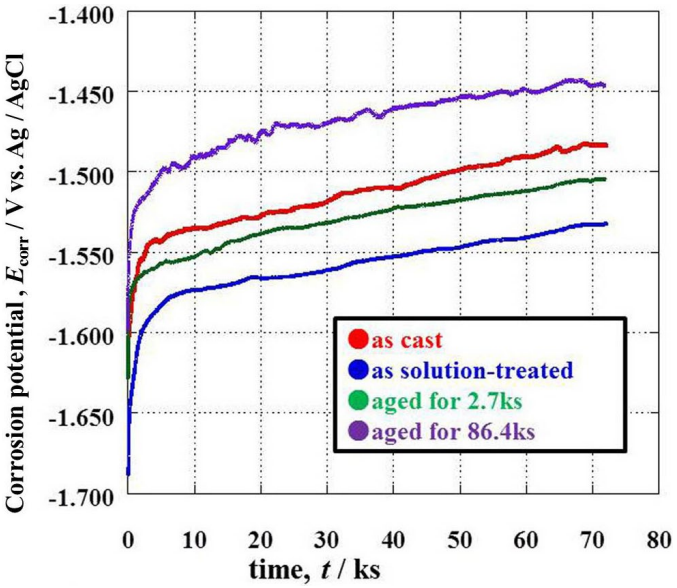

Fig. 3. OCP measurement with immerssion time, as a function of time for the Mg-9mass%Al alloys in 0.176 mol/dm^3 NaCl solution

that a stable film was formed and the thickness increased with the time in a similar manner also in this experiment. According to this result, measurements of polarization curve and EIS were started 12 ks after immersion as the OCP became stable.

3.3. Polarization curve measurements

Anodic polarization curves of the as-cast, the solution treated, the sub-aged and the peak-aged specimens are shown in Fig. 4. OCPs are –1.54 V for the as-cast, –1.58 V for the solution treated, –1.56 V for the sub-aged and –1.47 V for the peak-aged specimens. When the OCP of the solution treated specimen without the β phase is takes as the reference, comparison of polarization curves of the aged specimens shows that the OCP increases in the order of the sub-aged, the as-cast and the peak-aged, the increase in the latter is substantial. Namely, E_{corr} increases with the β phase content. Cathodic polarization curves are shown in Fig. 5. The corrosion current density I_{corr} was calculated for measured cathodic polarization curves using the Tafel extrapolation method [23]. Corrosion current densities were 0.271 A/m^2 for the as-cast, 0.215 A/m^2 for the solution treated, 0.251 A/m^2 for the sub-aged and 0.096 A/cm^2 for the peak-aged specimens. Corrosion rate of these alloys were estimated from the I_{corr}. Corrosion rate of these alloys were 0.536 mm/y for the as-cast, 0.426 mm/y for the solution treated, 0.497 mm/y for the sub-aged and 0.190 mm/y for the peak-aged specimens. Relationship between corrosion current density I_{corr} and area rate of the β and lamellar phase is shown in Fig. 6. Fig. 6 indicates that the corrosion current density is low in the peak-aged or in the solution treated specimen having single phase (unipolarity).

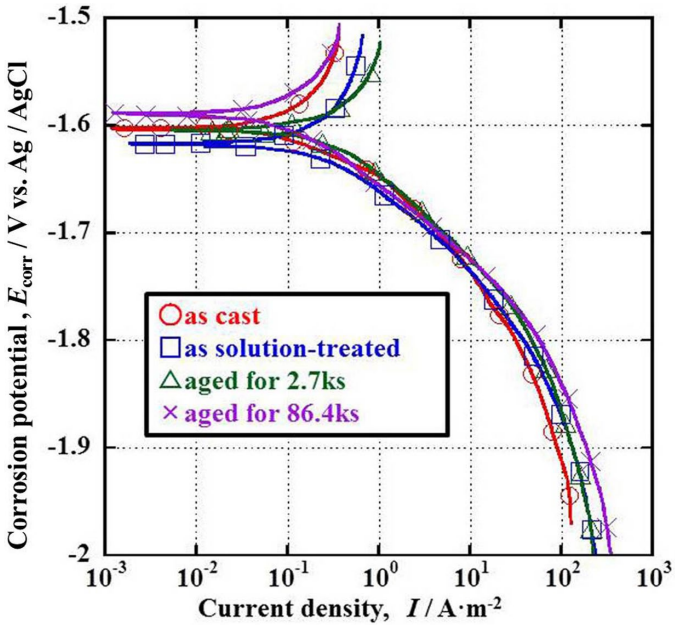

Fig. 4. Anodic polarization curves of the AM90 alloy measured in 0.176 mol/dm^3 NaCl solution at 298 K

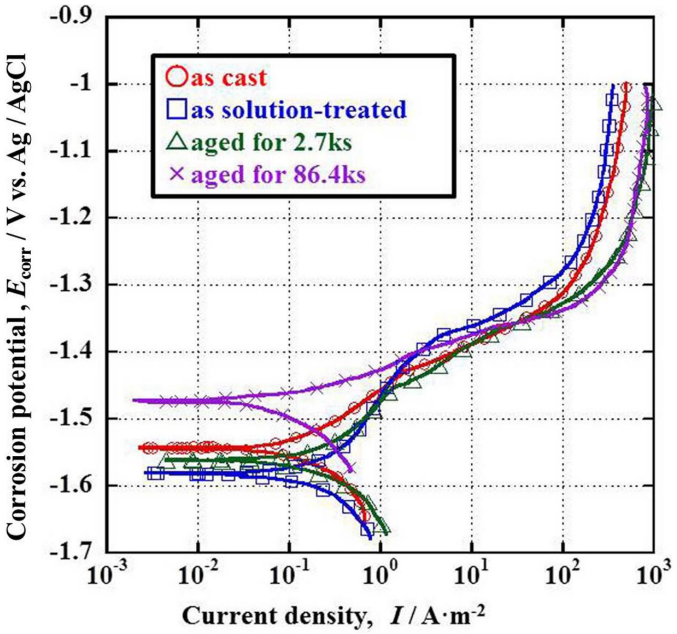

Fig. 5. Cathodic polarization curves of the AM90 alloy measured in 0.176 mol/dm^3 NaCl solution at 298 K

On the other hand, it is higher in the as-cast or in the sub-aged specimen having two phases of microstructure (bipolarity). Electrochemical impedance measurements were attempted to investigate the difference in corrosion current densities in detail in spite of having the same chemical composition.

3.4. Electrochemical impedance tests

Electrochemical impedance measurements were carried out to examine the results of polarization curve measurements in more detail. Locus of electrochemical impedance measurements was presented in an impedance diagram. It is constituted of three semi-circles as shown in Fig. 7 schematically. The first capacitive semi-circle in the first quadrant represents the charge transfer resistance R_{ct} and the electric double-layer capacitance C_{dl}. The second capacitive semi-circle is associated with the formation of protective film. The third capacitive semi-circle in the fourth quadrant is attributable to the anodic dissolution via an intermediate attracting body associated with dissolution of the protective film. Here, the charge transfer resistance R_{ct} corresponding to a diameter of the capacitive semi-circle in the first quadrant was calculated for each set potential according to the equation (1) given by Sunada et al. [24]. The model includes two relaxation processes of Z_1 and Z_2 is based on the Kendig's paper [25].

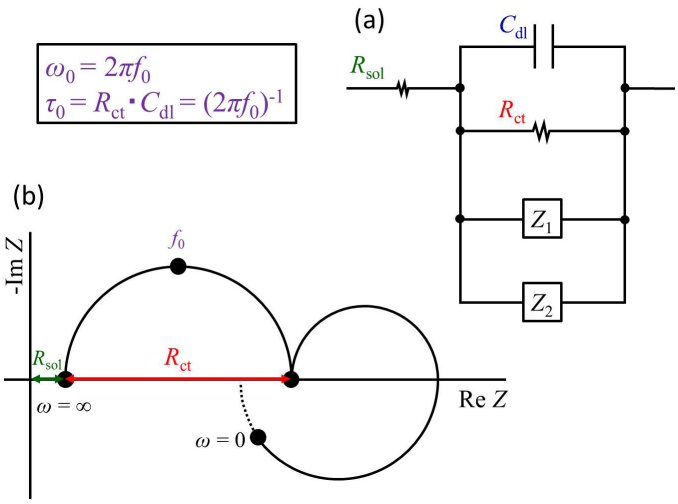

Fig. 6. Relationship between I_{corr} and area rate of the β and lamellar phase

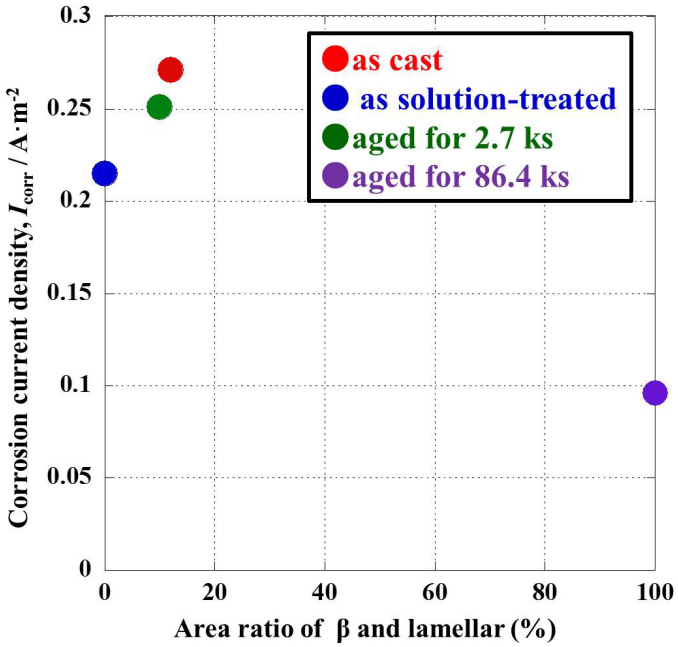

Fig. 7. (a) Equivalent circuit of the passive AM90 electrode. R_{sol}: Solution resistor. (b) Cole-Cole plot of impedance vectors in Equivalent circuit of (a)

$$\frac{1}{Z}=\frac{1+(j\omega\tau_0)^{\gamma}}{R_{ct}}+\frac{1}{Z_1}+\frac{1}{Z_2}$$
$$\frac{1}{Z}=\frac{1+(j\omega\tau_0)^{\gamma}}{R_{ct}}+\frac{1}{R_1(1+j\omega\tau_1)}+\frac{1}{R_2(1+j\omega\tau_2)} \quad (1)$$
$$\tau_0=R_{ct}\cdot C_{dl}=(2\pi f_0)^{-1},\ \omega=2\pi f$$

where γ – Electrode roughness constant (0.7-0.9).

Fig. 8 shows the relationships between the corrosion resistance and R_{ct} for each specimen all at once graphically. Rainbow curves with steep gradient are seen in all specimens in Fig. 8. EIS results of heat treated AM90 alloys are summarized in TABLE 2. Specimen-by-specimen comparison of R_{ct} at E_{corr} shows that the maximum value of R_{ct} is higher in the peak-aged specimen and that is lower in the as-cast and in the sub-aged specimens. It indicates that the higher the R_{ct}, the more corrosion resistive it is. Due to the above results, it can be said that the as-cast and the sub-aged specimens having two phases in microstructure show poor corrosion resistance and the heat treated and the peak-aged specimens consist of single phase microstructure show preferable corrosion resistance. The result of the corrosion resistance by electrochemical impedance measurements coincides with the tendency of the corrosion current density obtained by polarization curve measurements. Volume fraction of the β phase and the morphology of the specimen are thought to be influential factors on the difference of corrosion resistance after microstructural change by the heat treatment.

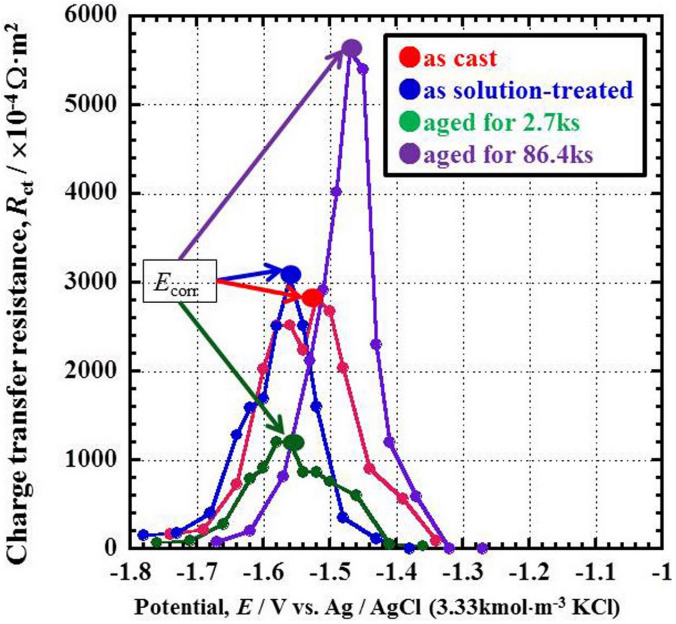

Fig. 8. Relationship between potential and charge transfer resistance

TABLE 2

EIS results of heat treated AM90 alloys

	E (V)	R_{ct} (×10^{-4} Ω·m^2)
as cast	–1.52	2834
solution treated	–1.56	3051
aged for 2.7ks	–1.56	1205
aged for 86.4ks	–1.47	5614

3.5. Potentiostatic corrosion tests with constant electric charges

Potentiostatic corrosion tests were carried out to clarify the reason of difference in a corrosion current density or corrosion resistance revealed in the polarization curve measurements and the impedance measurements in spite of the same composition of the specimens. Fig. 9 shows cross-sectional surface of Mg-9mass%Al alloy corroded with the charge density of 5 C/cm^2. Matrix of the primary crystal α phase and the β phase distributed at the grain boundaries are observed in the as-cast specimen. The α phase appearing white around the β phase dissolves preferentially. It shows that the β phase remains due to its low corrosion current density. Next, partially rounded pitting corrosions were observed in the solution treated specimen. As it has a single phase structure of the α phase, characteristic behaviors such as preferential dissolution were not observed. Lamellar precipitates remained in the sub-aged specimen and the surrounding α phase dissolved preferentially. Preferential dissolution of the α phase is also attributable to the lower corrosion current density of the lamellar precipitate than that of the α phase. The peak-aged specimen was corroded uniformly. Thus, there are various corrosion morphologies.

3.6 Cathodic polarization curve after application of 5 C/cm^2 charges

Cathodic polarization curves were measured on a specimen with the exposed β phase to examine a role of the β phase after application of 5 C/cm^2 charges. Obtained values of the E_{corr}, I_{corr} and corrosion rate of examined specimens with and without 5 C/cm^2 charges are summarized in the TABLE 3. Fig. 10 shows the relationships between the area rate of the β and lamellar phase and the corrosion current density I_{corr} calculated from polarization curve of the specimen after application of 5 C/cm^2 and that without 5 C/cm^2 charge. Fig. 10 shows that the corrosion current density after 5 C/cm^2 application is 1.3 times higher than that without 5 C/cm^2 charge in the single phase solution treated specimen and this gap becomes 2.5 times in the peak-aged specimen. These changes are relatively small. On the contrary, in case of the specimens having two phases, the gaps become 6.3 times and 4.5 times higher in the as-cast and in the sub-aged specimens respectively. According to the Cross-sectional micro-graphs of the Mg-9mas% Al alloys, after 5 C/cm^2 corrosion test of Fig. 9, large dissolution of the α phase around the β phase was observed in the specimens having two phases, and it is considered that this phenomenon increased the actual area ratio of the β phase and the dissolution of the α phase increased the I_{corr}, in such cases. The relationships between the area rate of the β and lamellar phase and the corrosion potentials measured after application

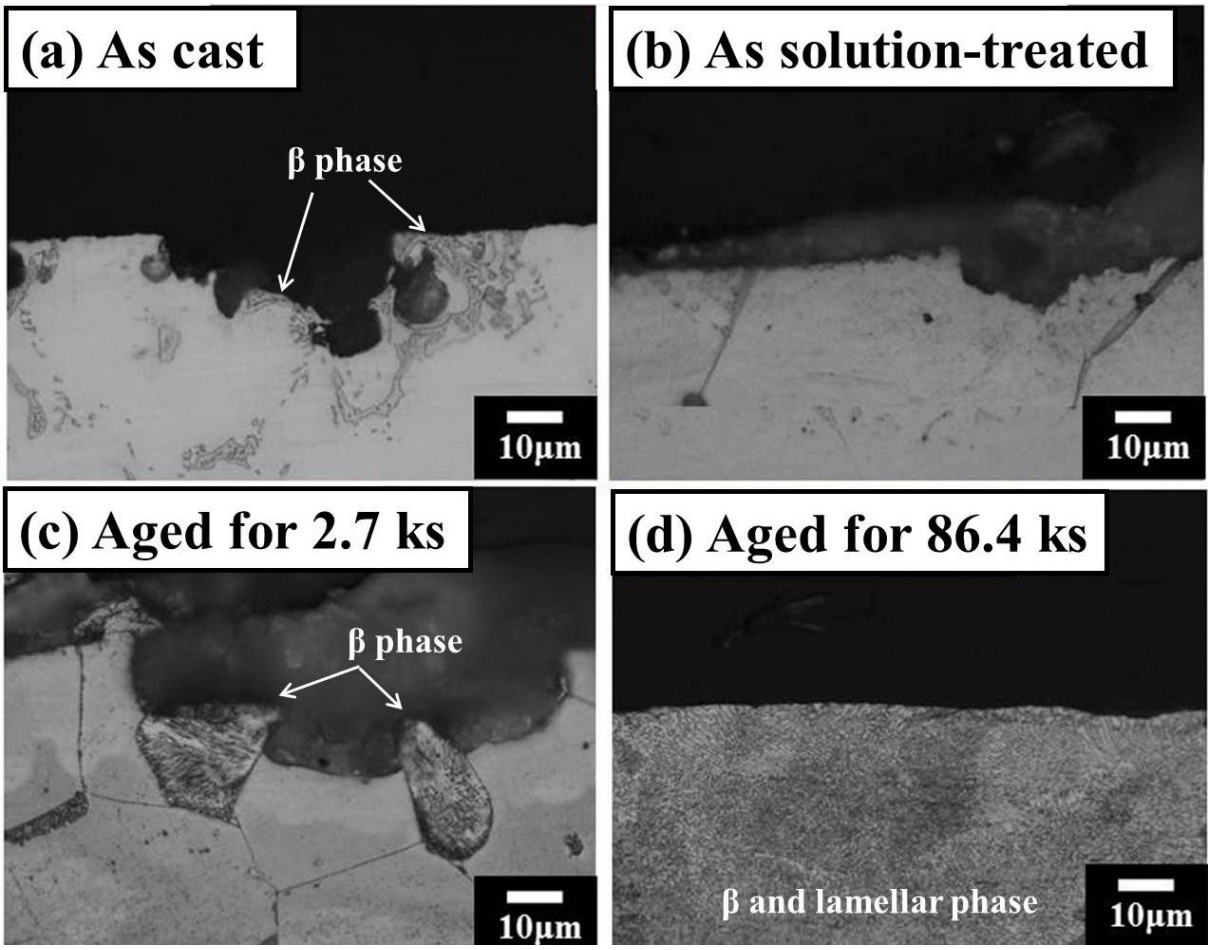

Fig. 9. Cross-sectional micro-graphs of the Mg-9mas% Al alloys, after 5 C/cm^2 corrosion test in 0.176 mol/dm^3 NaCl solution at 298 K

of 5 C/cm^2 charges and those without 5 C/cm^2 charges are shown in Fig. 11. Surges of E_{corr} are shown in both the as-cast and the sub-aged specimens having two phases. E_{corr} is small in the single phase solution treated specimen on the other hand. Based on surges of the corrosion potential E_{corr} and increases in the corrosion current density I_{corr} in the as-cast and the sub-aged specimens having two phases, it can be concluded that the β phase acts as a cathodic electrode and the cathodic reaction is accelerated. In the case of peak-aged specimen, lamellar phase seemed to be shown such phenomena. However, β phase might

TABLE 3

OPC results of heat treated AM90 alloys with and without application of 5 C/cm^2 charges

		E_{corr} / V vs. Ag/AgCl	I_{corr} / A·m^{-2}	Corrosion rate, mm / y
As cast		–1.602	0.271	0.536
	after 5 C/cm^2	–1.584	1.710	3.390
As solution-treated		–1.618	0.215	0.426
	after 5 C/cm^2	–1.608	0.214	0.424
Aged for 2.7 ks		–1.604	0.251	0.497
	after 5 C/cm^2	–1.590	1.120	2.220
Aged for 86.4 ks		–1.580	0.096	0.190
	after 5 C/cm^2	–1.577	0.237	0.496

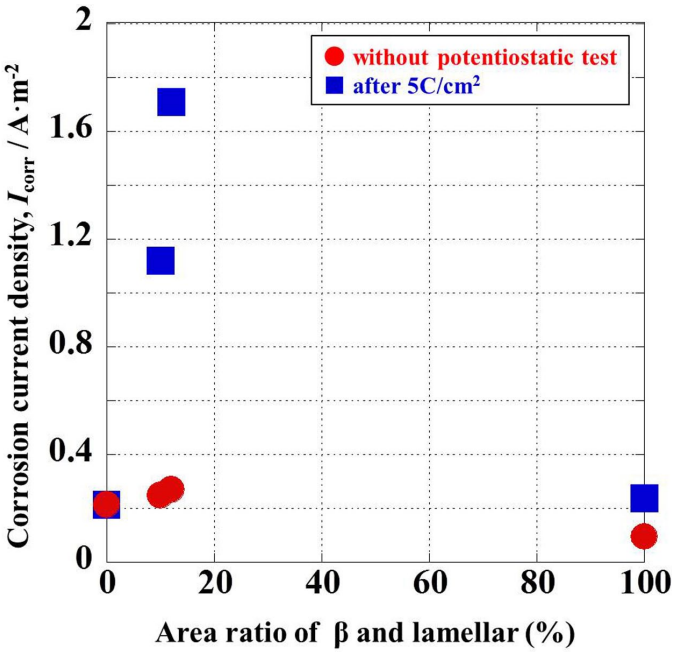

Fig. 10. Relationship between I_{corr} and area ratio of β and lamellar phase

act as an anodic barrier to inhibit the overall corrosion of the alloy. The increase in I_{corr} after the 5 C/cm^2 charges is slightly suppressed to 2.5 times, and the corrosion rate is small.

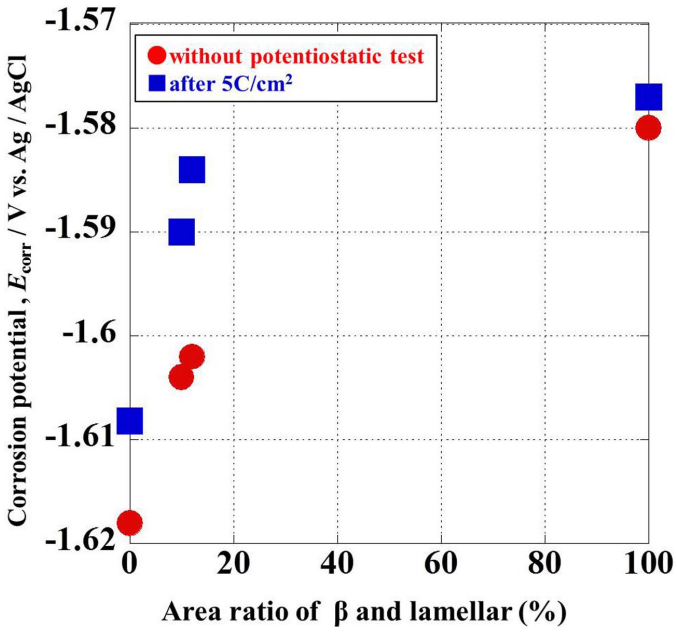

Fig. 11. Relationship between E_{corr} and area ratio of β and lamellar phase

4. Conclusions

From the results of this work, following conclusions have been drawn experimentally.

(1) The volume fraction of the β phase influences remarkably on corrosion current density and corrosion resistance in AM-90 alloy. Based on measurements of electrochemical impedance and polarization curve, it was extruded that the as-cast or the sub-aged alloy having precipitated β phase shows poor corrosion resistance and the single phase alloy like the peak-aged or the solution treated alloy shows excellent corrosion resistance.

(2) The corrosion current density of the β and lamellar phase alloy was evaluated. It was shown quantitatively that its corrosion resistance is smaller than that of the α phase.

(3) Positive correlation between the area rate of the β and lamellar phase and the open circuit potential E_{corr} indicates that the β phase acts as a cathodic electrode.

(4) The β phase is also thought to act as a cathode electrode based on accelerated cathodic reaction and the relative increases in corrosion current density of the as-cast and the sub-aged alloys with larger area of exposed β phase after application of 5 C/cm^2 charges.

Acknowledgements

This study was financially supported by JSPS KAKENHI Grant Number JP 18K04774.

REFERENCES

[1] B.L. Mordike, T. Ebert, Materials Science and Engineering A **302**, 37-45 (2001).
[2] Y. Mori, A. Koshi, J. Liao, Corr. Sci. **104**, 207-216 (2016).
[3] S. Seetharaman, C. Blawert, B.M. Ng, W.L.E. Wong, C.S. Goh, N.H., M. Gupta, J. Alloys. Compd. **648**, 759-770 (2015).
[4] B. Mingo, M. Mohedno, C. Blawert, R. del Olmo, N. Hort, R. Arrabal, J. Alloys. Compd. **811**, 151992 (2019).
[5] L. Zhang, Z.Y. Cao, Y.B. Liu, G.H. Su, L.R. Cheng, Mater. Sci. Eng. A **508**, 129-133 (2009).
[6] M. Esmaily, M. Shahabi-Navid, J.-E. Svensson, M. Halvarsson, L. Nyborg, Y. Cao, L.G. Johansson, Corr. Sci. **90**, 420-433 (2015).
[7] K.R. Gopi, H.S. Nayaka, S. Sahu, Arab. J. Sci. Eng. **43**, 4871-4878 (2018).
[8] Z. Shin, G. Song, A. Atrens, Corr. Sci. **48**, 3531–3546 (2006).
[9] M. Furui, S. Saitou, S. Sunada, S. Saikawa, J. J. Inst. Light Metals **60**, 629-634 (2010).
[10] R. Raman, Metall. Mater. Trans. A **35**, 2525-2531 (2004).
[11] Y. Ishibashi, M. Nose, M. Hatakeyama, S. Sunada, Arch. Metal. Mater. **60**, 953-955 (2015).
[12] M. Hatakeyama, K. Shimono, D. Iwashima, S. Saikawa, S. Sunada, Arch. Metal. Mater. **62**, 155-158 (2017).
[13 G.L. Song, A. Atrens, Adv. Eng. Mater. **1**, 11(1999).
[14] A. Pardo, M.C. Merino, A.E. Coy, R. Arrabal, F. Viejo, E. Matykina, Corr. Sci. **50**, 823-834 (2008).
[15] P. Casajus, N. Winzer, Corr. Sci. **94**, 316-326 (2015).
[16] E. Koç, Acta Physica Polonica A, 135 (2019) 881-883.
[17] S. Al. Bacha, I. Aubert, O. Devos, M. Zakhour, M. Nakhl, J.-L. Bobet, Int. J. Hydrog. Energy **45**, 15805-15813 (2020).
[18] M. Grimm, A. Lohmüller, R.F. Singer, Sannakaisa Virtanen, Corr. Sci. **155**, 195-208 (2019).
[19] S. Sunada, A. Takagi, M. Hatakeyama, J. Umeda, K. Kondo, Chiang Mai J. Sci. **43**, 381-392 (2016).
[20] R.M. Wanga, A. Eliezerb, E.M. Gutmanb, Mater. Sci. Eng. A. **25**, 201-207 (2003).
[21] P. Casajus, N. Winzer, Corr. Sci. **94**, 316-326 (2015).
[22] N. Hara, Y. Kobayashi, D. Kagaya, N. Akao, Corr. Sci. **49**, 166-175 (2007).
[23] J. Tafel, Z. Physik. Chem. **50**, 641 (1905).
[24] S. Sunada, T. Yamamoto, K. Majima, N. Nunomura, J. Jpn. Soc. Powder Metal. **52**, 551-561 (2005).
[25] M.W. Kendig, E.M. Meyer, G. Lnidberg, F. Mansfeld, Corr. Sci. **23**, 1007-1015 (1983).